https://doi.org/10.26599/FRICT.2026.9441305

Research Article

# Tribochemical and tribomechanical effect of $TiO_2$ nanoparticle: Different influence on MoDTC and ZDDP additives

Zhikai Fan[a], Shanshan Wang[b], Xiangyu Ge[a], Yanfei Liu[a, c *], Wenzhong Wang[a]

a School of Mechanical Engineering, Beijing Institute of Technology, Beijing, China

b Analysis & Testing Center, Beijing Institute of Technology, Beijing, China

c Tangshan Research Institute, Beijing Institute of Technology, Tangshan, China

* Corresponding author. E-mail addresses: liuyanfei@bit.edu.cn (Y. Liu).

Received: May 14, 2026; Revised: July 21, 2026; Accepted: August 23, 2026





**Abstract**

This study investigates the formulation-dependent tribochemical regulation of $TiO_2$ nanoparticles in molybdenum dithiocarbamate (MoDTC), zinc dialkyldithiophosphate (ZDDP), and their blended lubricant systems. Reciprocating ball-on-disk tribological tests were conducted under a normal load of 20 N, corresponding to Hertzian contact pressure of 1.33 GPa. $TiO_2$ nanoparticles promoted $MoS_2$-rich tribofilm formation in the lubricant with single MoDTC, which led to reduction of both the coefficient of friction and wear of counterparts. Conversely, in the MoDTC-ZDDP blended system, $TiO_2$ drove interfacial reactions toward high-valence Mo oxides and sulfate species, leading to increased wear. Atomic force microscope measurements confirmed that protruded $MoS_2$-rich tribofilm formed by lubricant containing MoDTC and $TiO_2$ exhibited low shear strength, whereas the protruded oxide/sulfate-rich tribofilm formed by lubricant containing MoDTC-ZDDP and $TiO_2$ generated higher local friction. These findings reveal that $TiO_2$ nanoparticles function as selective tribochemical regulators whose effects are governed by interfacial reaction competition and additive compatibility, rather than universally enhancing lubrication performance. This work provides critical mechanistic insights for rational design of nanoparticle-modified lubricant formulations.

**Keywords:** $TiO_2$ nanoparticles; MoDTC; ZDDP; Tribofilm; Tribochemistry



## 1. Introduction

Friction and wear are ubiquitous in the critical moving interfaces of mechanical equipment and are major contributors to energy loss, component failure, and reduced service life[1]. It has been reported that a substantial proportion of global energy consumption is associated with frictional contacts and wear-induced failures. Therefore, reducing friction and wear through lubrication technologies is of great significance for improving the energy efficiency, reliability, and service life of mechanical systems [2]. Under boundary lubrication conditions, lubricating oils are unable to form a complete fluid lubricating film, and the friction-reducing and anti-wear performance of the sliding interface mainly depends on tribochemical films formed by lubricant additives under friction-induced reactions [3]. Therefore, developing lubricant additive systems capable of effectively regulating interfacial reaction processes and promoting the formation of high-performance tribofilms is essential for improving the operational efficiency and service reliability of mechanical systems.

With the development of advanced equipment toward higher efficiency, longer service life, and low-carbon operation, lubricant additives are required not only to provide excellent lubrication and anti-wear performance but also to meet the demands of environmental friendliness and sustainable development [4, 5]. Although conventional lubricant additives have a well-established engineering application basis, their long-term use may raise concerns related to emissions, ash formation, and environmental compatibility [6-8]. Therefore, alternative additive systems with low dosage, high efficiency, and good environmental compatibility have attracted increasing attention. Nanomaterials, including graphene [9-11], $MoS_2$, MXenes [12], nanodiamonds [13, 14], etc., have been demonstrated to effectively improve the lubrication and anti-wear performance of lubricants. Metal oxide nanoparticles can enhance tribological performance through micro-filling [15], rolling effects [16], and tribochemical regulation [17] due to their high specific surface area, good chemical stability, and interfacial activity [18, 19].In addition, the low cost of metal oxides further promotes their engineering application. Among the metal oxide nanomaterials, $TiO_2$ nanoparticles are widely available, chemically stable, and relatively environmentally friendly, showing promising application potential as green nanolubricant additives [20].

ZDDP is one of the most widely used anti-wear additives and can form protective films containing Zn, P, S, and O at friction interfaces, thereby suppressing direct metal-to-metal contact and wear [21-24]. Differently, MoDTC is a typical organomolybdenum friction modifier that can generate low-shear species such as $MoS_2$ during sliding, thereby significantly reducing interfacial friction [25-27]. However, the tribochemical reaction process of MoDTC is strongly affected by temperature, counterface material, and coexisting additives, etc. The relative proportions of $MoS_2$, $MoO_3$, and other Mo-containing species in its reaction products play a decisive role in the lubrication effectiveness of the tribofilm [28, 29]. Because MoDTC primarily functions as a friction modifier, whereas ZDDP mainly provides anti-wear protection, their combination is considered an important strategy for improving the overall performance of lubricants [30, 31]. Morina et al. [30] investigated the frictional behavior of PAO6 containing both ZDDP and MoDTC using a reciprocating pin-on-disk tribometer. Their results showed that the tribofilm generated from ZDDP interacted with the molybdenum oxides formed from MoDTC, leading to a reduction in molybdenum oxide species and thereby achieving improved friction performance.

However, the combined action of MoDTC and ZDDP is not a linear superposition of their individual effects. At the friction interface, they may undergo complex interactions, including competitive adsorption, reaction coupling, and tribofilm structural reconstruction, thereby influencing the formation of tribochemical products such as $MoS_2$, molybdenum oxides, phosphates, and sulfates. When nanoparticles are further introduced into such blended systems, additional interfacial active species are involved, making the interfacial reaction pathways even more complex. Previous studies have shown that $TiO_2$ nanoparticles at appropriate concentrations can synergistically interact with MoDTC, promoting the formation of Mo-containing tribofilms and improving friction and wear performance [17]. However, whether $TiO_2$ nanoparticles exert the same promoting effect on MoDTC-ZDDP blended systems, as well as their influence pattern and underlying mechanism, remains to be further clarified. Therefore, elucidating the differential effects of $TiO_2$ nanoparticles on different lubricant additives is of great significance for the formulation design of advanced lubricants.

Based on this, a series of lubricants containing MoDTC, ZDDP, MoDTC-ZDDP, and their combinations with $TiO_2$ nanoparticles were prepared. The effects of $TiO_2$ nanoparticles on the tribological performance of different lubricants were systematically investigated. By establishing correlations among lubricant composition, tribological behavior, tribofilm structure, and interfacial reaction mechanisms, this study reveals the differential regulatory mechanisms of $TiO_2$ nanoparticles toward MoDTC, ZDDP, and MoDTC-ZDDP blended systems. The findings of this study provide insights and guidance for the formulation design of high-performance lubricants.

## 2. Experimental materials and methods

### *2.1. Materials*

In this study, PAO4 base oil (Dowpol Chemical International Corp., China) was used as the lubricant matrix. MoDTC (MOLYVAN-3000, Vanderbilt, USA), ZDDP (Shandong Weifang Runfeng Chemical Corp., China), and $TiO_2$ nanoparticles (Shanghai Aladdin, China) were selected as functional lubricant additives. During lubricant preparation, $TiO_2$ nanoparticles were first dispersed in PAO4 by ultrasonication for 2 h to obtain a homogeneous nanolubricant. The nanoparticle concentration was fixed at 5 mg/mL. MoDTC and ZDDP were then added at predetermined concentrations, followed by an additional 30 min of ultrasonication to ensure adequate dispersion and mixing of the additive components. For clarity in the following discussion, different lubricant formulations are denoted by specific abbreviations, as listed in Table 1.

**Table 1**. Abbreviations of the lubricant formulations.

| Different lubricant formulations | Abbreviation |
| --- | --- |
| PAO4+2 wt% MoDTC | PAO4_MoDTC |
| PAO4+2 wt% MoDTC+5 mg/mL $TiO_2$ | MoDTC_$TiO_2$ |
| PAO4+2 wt% ZDDP | PAO4_ZDDP |
| PAO4+2 wt% ZDDP+5 mg/mL $TiO_2$ | ZDDP_$TiO_2$ |
| PAO4+1 wt% MoDTC+1 wt% ZDDP | MoDTC_ZDDP |
| PAO4+1 wt% MoDTC+1 wt% ZDDP+5 mg/mL $TiO_2$ | MoDTC_ZDDP_$TiO_2$ |

The lubricants were prepared as follows. $TiO_2$ nanoparticles were first dispersed in

PAO4 base oil by ultrasonication for 2 h to obtain a homogeneous nanolubricant. Based on our previous study [17], the $TiO_2$ nanoparticle concentration was set at 5 mg/mL, which was found to provide the best lubrication and wear-resistance performance in combination with MoDTC. MoDTC and ZDDP were then introduced at predetermined mass fractions, followed by an additional 30 min of ultrasonication to ensure thorough dispersion (Fig. 1a). It has been reported that the synergistic effect of MoDTC and ZDDP promotes $MoS_2$ formation on the rubbing surface, thereby enhancing tribological performance. [31, 32] Accordingly, the $TiO_2$ concentration was optimized with respect to the MoDTC-containing system.

*2.2. Tribological tests*

To investigate the regulatory effect of $TiO_2$ nanoparticles on the MoDTC and ZDDP blended additive system, tribological tests were performed to systematically evaluate the friction and wear performance of different lubricants. The tests were conducted under a reciprocating ball-on-disk contact configuration using a UMT-3 tribometer (Bruker, USA).

Tribological tests were performed under normal load of 20 N, corresponding to Hertzian contact pressure of 1.33 GPa. The ambient temperature and relative humidity were maintained at 25 ± 2°C and 34 ± 3%, respectively. The tribological pair consisted of AISI 52100 bearing steel plates (25 mm × 25 mm × 3 mm) as the lower specimens and AISI 52100 steel balls (9.525 mm in diameter) as the upper counterparts. The surface roughness values (Ra) of the steel plates and balls were approximately 14 and 4 nm, respectively. For each tribological test, 30 μL of lubricant was applied. During testing, the reciprocating stroke length and frequency were set to 4 mm and 3 Hz, respectively, corresponding to a linear sliding speed of approximately 0.024 m/s. The schematic illustration of the tribological test configuration is shown in Fig. 1b. To ensure the reliability and repeatability of the experimental results, each test was repeated at least three times, and the average values were used for subsequent analysis.

*2.3. Surface characterization*

After the 1800 s tribological tests, the worn surfaces were cleaned with anhydrous ethanol to remove residual lubricant and loosely attached contaminants. The wear scars were first observed using optical microscopy. The wear volume of the steel balls was quantified using a three-dimensional white-light interferometer (Nexview, ZYGO). The surface morphology of the worn regions was further examined by scanning electron microscopy SEM; (S-4800, Hitachi High-Technologies Corporation, Japan), and the elemental distributions were analyzed using an energy-dispersive X-ray spectroscopy detector coupled with the SEM (EDS; NORAN SYSTEM 7, Thermo Fisher Scientific, Inc., USA). X-ray photoelectron spectroscopy (XPS, PHI Quantera II) was further employed to analyze the tribochemical reaction products formed on the steel ball surfaces, thereby revealing the sliding friction-induced changes in chemical states. The schematic illustration of the corresponding characterization workflow is shown in Fig. 1c.

*2.4. Functional mechanism validation with microscale friction tests*

Atomic force microscopy (AFM, Oxford Instruments MFP-3D) was used to measure the local friction force of the tribofilms formed on the wear scars of the steel balls, with the aim of elucidating the microscale shear frictional characteristics of tribofilms generated by different lubricants systems and their correlation with the macroscopic tribological behavior. The AFM friction tests were conducted in contact mode using a conventional Bruker MLCT-SPH-1UM probe. The tribofilm surfaces were scanned over an area of 1 μm × 0.2 μm at a frequency of 1 Hz. During AFM friction measurements, the friction signal output by the instrument essentially corresponds to a voltage response induced by the lateral torsion of the microcantilever. Therefore, lateral force calibration using a wedge calibration grating was required to convert the voltage signal into friction force and friction coefficient values with clear physical meaning. A TGF11 wedge calibration grating was first used to calibrate the lateral force response of the AFM probe. During wedge calibration, lateral scanning signals were collected under different normal loads, and the geometric features of the inclined planes of the calibration grating were used to establish the relationship between the lateral voltage signal and the actual lateral force. The lateral force calibration coefficients under different loads were then obtained accordingly. Considering that AFM lateral force measurements are highly sensitive to the probe condition, laser position, and testing parameters, all subsequent sample measurements were performed using the same probe and parameter settings as those used during calibration. This ensured the applicability of the calibration coefficients and the comparability of the obtained results.

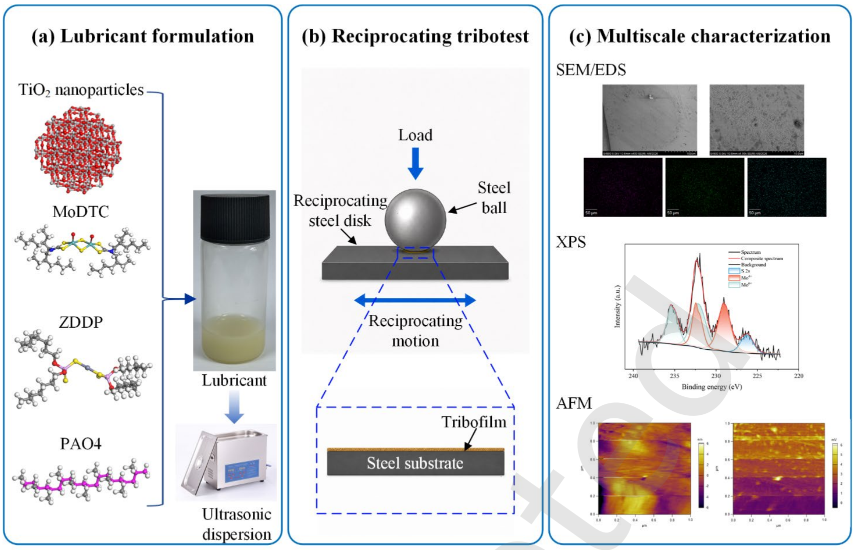


**Fig. 1**. Schematic illustration of (a) the lubricant preparation procedure, (b) the tribological test configuration, and (c) the subsequent characterization workflow.

## 3 Results and discussion

### *3.1 Tribological performance*

Tribological tests were performed using lubricants containing different additive systems to clarify the influence of $TiO_2$ nanoparticles on MoDTC, ZDDP, and blended MoDTC-ZDDP lubricants. Because the tribological performance of lubricant additives is governed by interfacial tribochemical reactions and the formation and stability of tribofilms, the friction-reduction and anti-wear behaviors of these lubricants were systematically compared under identical testing conditions. This comparison enables a direct evaluation of the formulation-dependent effect of $TiO_2$ nanoparticles on different lubricant additive systems.

The friction tests were conducted under a normal load of 20 N, corresponding to an average Hertzian contact pressure of 1.33 GPa. As shown in Fig. 2a, the coefficient of friction (COF) exhibited distinct time-dependent evolution with the lubrication of different lubricants. For PAO4_MoDTC, the COF rapidly decreased from a relatively high initial value to approximately 0.075 at the early stage of sliding and remained generally stable thereafter. This indicates that, under the 20 N normal load, MoDTC can rapidly participate in the interfacial lubrication process and establish a relatively stable low-friction state. After the introduction of 5 mg/mL $TiO_2$ nanoparticles, the frictional response of MoDTC_$TiO_2$ changed markedly. The COF quickly entered a stable regime during the initial stage; however, after stabilization, it gradually decreased with increasing sliding time. The COF stabilized at approximately 0.070 after about 200 s and then continued to decrease slowly, reaching approximately 0.057 toward the end of the test. These results suggest that the incorporation of $TiO_2$ nanoparticles further enhances the lubrication capability of the MoDTC-containing lubricant. As comparison, the friction curve of PAO4_ZDDP exhibited a markedly different evolution behavior. After a brief decrease at the initial stage, the COF rapidly stabilized at approximately 0.100 and remained at a relatively high level throughout the 1800 s test, with only slight fluctuations. Upon further incorporation of $TiO_2$ nanoparticles, the COF curve of ZDDP_$TiO_2$ was generally higher than that of PAO4_ZDDP, with a steady-state COF of approximately 0.105–0.110. The COF remained high even at the later stage of the test, indicating that the addition of $TiO_2$ nanoparticles did not improve the lubrication behavior of PAO4_ZDDP but instead led to an increase in friction.

For the MoDTC_ZDDP blended lubricant, the COF rapidly decreased to approximately 0.067 at the initial stage of the test. However, this low-friction state was not sustained. Instead, the COF gradually increased during the period of approximately 300–800 s and eventually stabilized at 0.072–0.074. In contrast, MoDTC_ZDDP_$TiO_2$ exhibited a relatively high initial COF of approximately 0.110, which then rapidly decreased to around 0.095. During subsequent sliding, the COF continued to decrease, with a more pronounced reduction observed after approximately 400 s. It decreased below 0.060 at around 900–1000 s and finally stabilized at approximately 0.055. These results indicate that, upon the incorporation of $TiO_2$ nanoparticles into the MoDTC_ZDDP blended lubricant, the formation of a tribofilm capable of reducing macroscopic friction requires a relatively prolonged running-in process, but eventually leads to a stable low-friction state.

As shown in Fig. 2b, PAO4_ZDDP and ZDDP_$TiO_2$ exhibited the highest average COF values among all lubricants, indicating that the single ZDDP additive provided limited friction-reducing capability under the 20 N normal load. The incorporation of $TiO_2$ nanoparticles did not improve the lubrication performance of PAO4_ZDDP; instead, it led to a slight increase in the COF. The above trends can be further supported by the optical microscopy images of the wear scars on the steel balls. As shown in Fig. 2(c1), PAO4_MoDTC produced a well-defined wear scar with visible grooves inside the worn region. The wear scar diameter was approximately 320 μm, indicating that although the single MoDTC additive provided moderate friction-reducing capability, its anti-wear performance remained limited. For MoDTC_$TiO_2$ (Fig. 2(c2)), a relatively evident tribofilm was observed on the wear scar surface, and the wear scar diameter decreased to approximately 280 μm.

After the friction tests, the morphology of wear regions was observed using optical microscopy. As shown in Fig. 2(c1), PAO4_MoDTC produced a wear scar with visible grooves inside the worn region, where the wear scar diameter was approximately 320 μm. For MoDTC_$TiO_2$ (Fig. 2(c2)), a relatively evident tribofilm was observed on the wear scar surface; and the wear scar diameter decreased to approximately 280 μm, indicating that addition of $TiO_2$ nanoparticles promoted the formation of tribofilm and while suppress wear. With the lubrication of PAO4_ZDDP and ZDDP_$TiO_2$, grooves can be clearly observed on the wear scar surfaces, while tribofilm with high coverage on the worn surface could not be clearly observe from the optical image, as shown in Fig. 2(d1) and Fig. 2(d2). With the lubrication of MoDTC_ZDDP, the wear scar diameter was approximately 300 μm (Fig. 2(e1)). After the addition of $TiO_2$ nanoparticles, the MoDTC_ZDDP_$TiO_2$ showed a slightly larger wear scar diameter of approximately 315 μm, suggesting that $TiO_2$ nanoparticles did not significantly improve the anti-wear behavior of the MoDTC_ZDDP (Fig. 2(e2)). From the optical images of the wear scar with the lubrication of both MoDTC_ZDDP and MoDTC_ZDDP_$TiO_2$, tribofilm with high coverage can be all clearly observed on the worn surface.

Overall, the single ZDDP additive exhibited a relatively high coefficient of friction, and the incorporation of $TiO_2$ nanoparticles did not improve the friction-reducing performance. In contrast, MoDTC showed superior friction-reduction capability, which could be further enhanced by the addition of $TiO_2$ nanoparticles. The combination of MoDTC and ZDDP resulted in a synergistic friction-reducing effect, while the further introduction of $TiO_2$ nanoparticles into MoDTC_ZDDP led to prolonged running-in period and slightly lower steady-state COF.

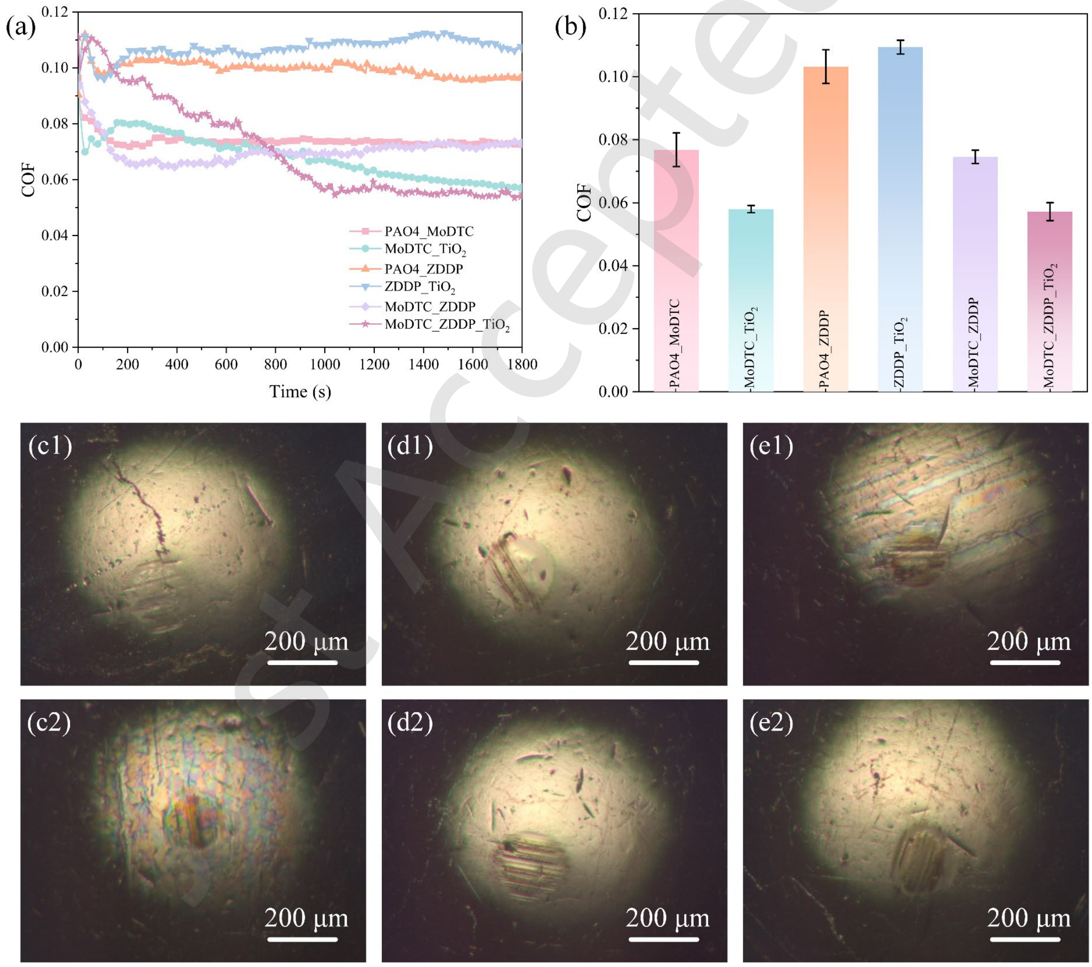


**Fig. 2**. Under a normal load of 20 N, tribological performance of different lubricants in the presence of $TiO_2$ nanoparticles: (a) coefficient of friction as a function of sliding time; (b) average coefficient of friction; optical microscopy images of the wear scars on steel balls lubricated with different formulations: (c1) PAO4_MoDTC, (c2) MoDTC_$TiO_2$, (d1) PAO4_ZDDP, (d2) ZDDP_$TiO_2$, (e1) MoDTC_ZDDP, and (e2) MoDTC_ZDDP_$TiO_2$. The error bars stand for the standard deviation of the results

acquired from independent tests.

To further quantitatively evaluate the anti-wear performance of different lubricants under a normal load of 20 N, three-dimensional white-light interferometry was employed to characterize the surface topography of the wear scars on the steel balls, based on the preceding analyses of COF evolution and optical wear scar morphology. The corresponding average wear volumes were then calculated from the wear scar profile data. By combining the white-light interferometric topographies with the volumetric wear loss results, the ability of different lubricants to suppress wear on the steel ball surfaces can be more directly assessed.

As shown in Fig. 3, the three-dimensional wear scar morphologies of the steel balls differed markedly among the lubricants, indicating their distinct protective capabilities for the steel surfaces. Under PAO4_MoDTC lubrication (Fig. 3a), wear can be significantly observed from the cross-sectional profile, although single MoDTC additive could suppress steel ball wear to a certain extent under the 20 N normal load. Compared with PAO4_MoDTC, the MoDTC_$TiO_2$-lubricated sample showed a smoother wear scar surface and a smaller wear depth (Fig. 3b), demonstrating that $TiO_2$ nanoparticles further improved the anti-wear performance of the lubricant.

For PAO4_ZDDP, the wear scar on the steel ball was relatively larger and exhibited a greater wear depth, indicating more severe wear (Fig. 3c). After introducing $TiO_2$

nanoparticles into the ZDDP-containing lubricant, the wear scar surface became smoother than that lubricated by PAO4_ZDDP, with a reduced wear depth (Fig. 3d). This indicates that $TiO_2$ nanoparticles effectively mitigated wear on the steel ball surface and improved the anti-wear performance of the ZDDP-containing lubricant. Figs. 3e and 3f show the three-dimensional wear scar morphologies and corresponding cross-sectional profiles of the steel balls lubricated with MoDTC_ZDDP and MoDTC_ZDDP_$TiO_2$, respectively. Under the 20 N normal load, the incorporation of $TiO_2$ nanoparticles into the MoDTC_ZDDP blended lubricant did not enhance the wear-resistance performance of MoDTC_ZDDP.

As shown in Fig. 3g, the wear volumes of the steel balls varied markedly among the different lubricants, reflecting significant differences in their anti-wear capabilities. Among them, MoDTC_$TiO_2$ exhibited the lowest average wear volume, approximately $2.6 \times 10^3$ $\mu m^3$, indicating the best anti-wear performance under the 20 N normal load. In comparison, PAO4_MoDTC showed a slightly higher average wear volume of approximately $3.4 \times 10^3$ $\mu m^3$, suggesting that the incorporation of $TiO_2$ nanoparticles further enhanced the anti-wear performance of MoDTC. PAO4_ZDDP exhibited the largest average wear volume, approximately $7.3 \times 10^3$ $\mu m^3$. This result indicates that the anti-wear performance of the single ZDDP additive was relatively weak. After the incorporation of $TiO_2$ nanoparticles, the average wear volume of ZDDP_$TiO_2$ decreased significantly to approximately $3.1 \times 10^3$ $\mu m^3$, demonstrating that $TiO_2$ nanoparticles markedly improved the anti-wear capability of the ZDDP-containing lubricant.

For the blended lubricants, MoDTC_ZDDP exhibited an average wear volume of approximately $3.7 \times 10^3$ μ$m^3$, which was slightly higher than those of PAO4_MoDTC and MoDTC_$TiO_2$ but significantly lower than that of PAO4_ZDDP. This indicates that the MoDTC-ZDDP blended additive maintained relatively stable anti-wear performance under the 20 N load. However, upon further incorporation of $TiO_2$ nanoparticles into MoDTC_ZDDP, the average wear volume of MoDTC_ZDDP_$TiO_2$ increased to approximately $5.9 \times 10^3$ μ$m^3$, which was markedly higher than that of MoDTC_ZDDP. This result suggests that the role of $TiO_2$ nanoparticles in the MoDTC-ZDDP blended system did not exhibit the same anti-wear enhancement observed in the lubricant with single additives.

Overall, the results in Fig. 3 indicate that, under the 20 N load, $TiO_2$ nanoparticles effectively enhanced the anti-wear performance of both MoDTC and ZDDP containing lubricants, as evidenced by the reduced wear scar size and decreased wear volume of the steel balls. However, in the MoDTC-ZDDP blended lubricant, the incorporation of $TiO_2$ nanoparticles was unfavorable for further improving the anti-wear performance.

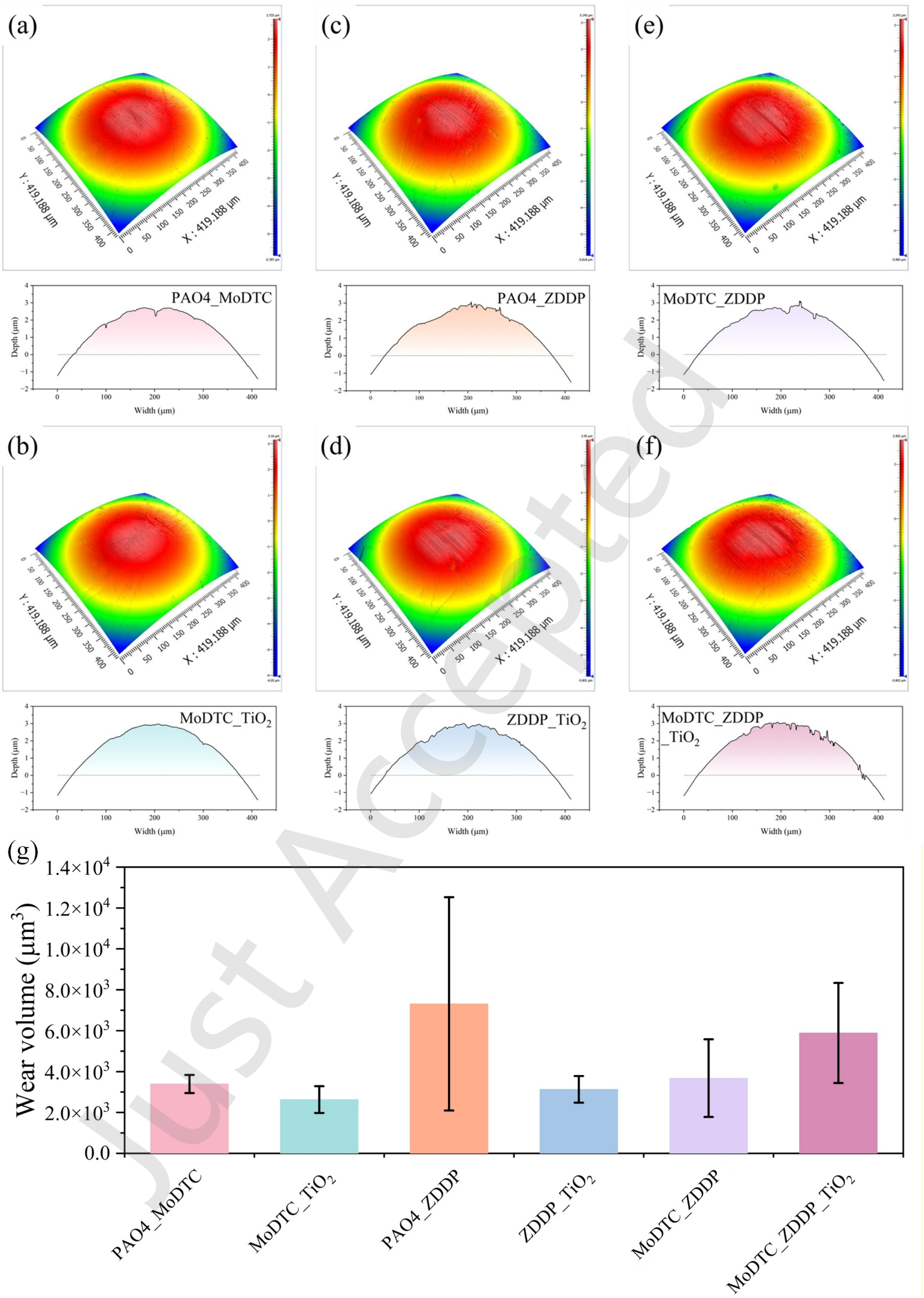


**Fig. 3**. Three-dimensional wear scar morphologies of the steel balls and the corresponding cross-sectional height profiles: (a) PAO4_MoDTC, (b) MoDTC_TiO$_2$, (c) PAO4_ZDDP, (d) ZDDP_TiO$_2$, (e) MoDTC_ZDDP, and (f) MoDTC_ZDDP_TiO$_2$; (g) average wear volume of the steel balls lubricated with different formulations. The error bars stand for the standard deviation of the results acquired from independent tests.

*3.2 Wear Scar Morphology and Elemental Distribution*

The tribological results demonstrate that, under a load of 20 N, the coefficient of friction and wear volume varied markedly among the different lubricant systems. To further elucidate the microstructural features of the wear scar surfaces formed under different lubricants and their relationship with the macroscopic tribological behavior, SEM and EDS analyses were performed on the wear scars of the steel balls. These analyses aimed to interpret the friction-reducing and anti-wear behavior of the different lubricant systems from the perspectives of surface morphology and elemental composition.

For the MoDTC-based lubricants, PAO4_MoDTC and MoDTC_$TiO_2$ showed markedly different wear scar features. Under PAO4_MoDTC lubrication, the wear scar exhibited obvious grooves along the sliding direction, together with local defects, fine pits, and discontinuous surface features, as shown in Fig. 4a and b. These features indicate that the tribofilm generated from MoDTC alone was not sufficiently continuous to fully protect the steel surface. This interpretation is supported by the EDS results in Fig. 4c, where the Fe content reached 90.20 wt%, while the Mo content was only 0.31 wt% and the S signal was relatively weak. The elemental maps in Figs. 4d–4h further show sparse and discontinuous distributions of Mo and S, suggesting limited formation and coverage of MoDTC-derived tribochemical products.

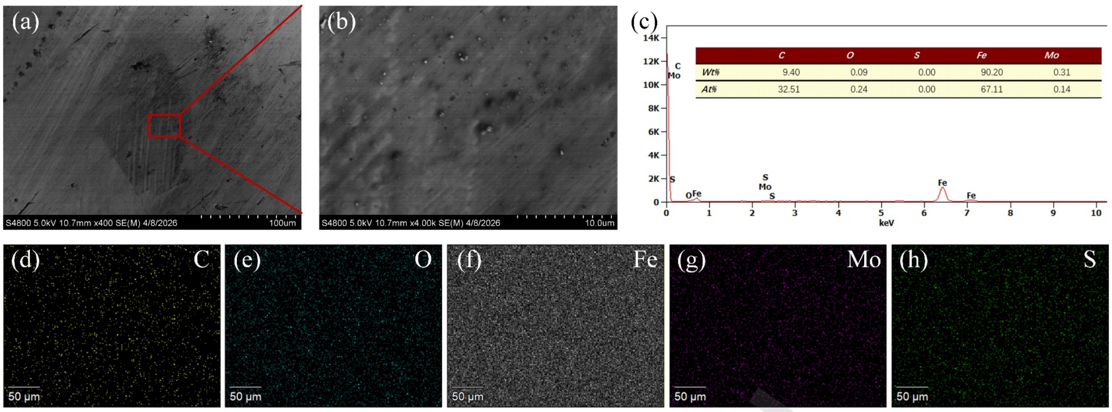


**Fig. 4**. SEM images of the wear scar surface on the steel ball lubricated with PAO4_MoDTC under a normal load of 20 N. (a) low-magnification and (b) high-magnification SEM images; (c) elemental contents in the wear scar region shown in (b); and corresponding EDS elemental maps of (d) C, (e) O, (f) Fe, (g) Mo, and (h) S.

After adding $TiO_2$ nanoparticles, the wear scar morphology became smoother and more uniform, with fewer local defects and less severe surface damage, as shown in Figs. 5a and 5b. The EDS results in Fig. 5c show that the Fe content decreased to 83.95 wt%, whereas the contents of O, S, Mo, and Ti increased to 2.71 wt%, 0.61 wt%, 1.54 wt%, and 0.16 wt%, respectively. Compared with PAO4_MoDTC, the pronounced increase in Mo and S contents, together with their more continuous distribution in Figs. 5d–5i, indicates that $TiO_2$ nanoparticles promoted the deposition and retention of MoDTC-derived tribofilm species on the wear scar surface. These results demonstrate that $TiO_2$ positively regulated MoDTC tribochemistry by enhancing the formation of Mo- and S-containing protective films.

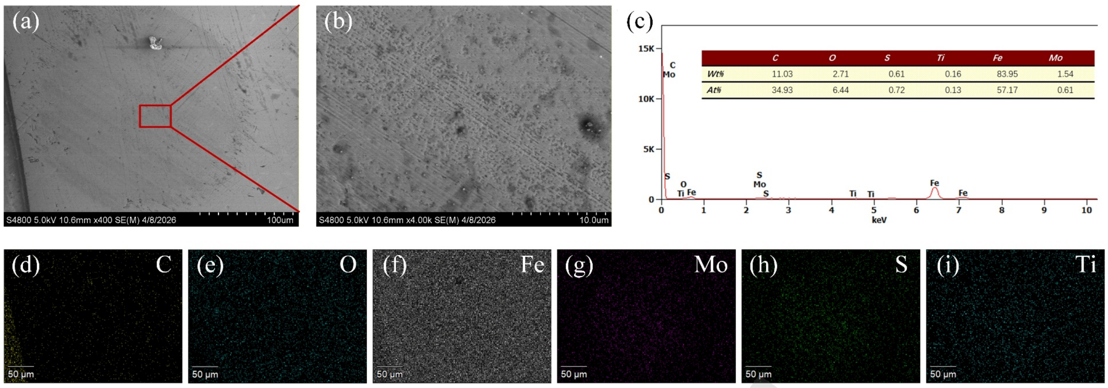


**Fig. 5**. SEM images of the wear scar surface on the steel ball lubricated with MoDTC_$TiO_2$ under a normal load of 20 N. (a) low-magnification and (b) high-magnification SEM images; (c) elemental contents in the wear scar region shown in (b); and corresponding EDS elemental maps of (d) C, (e) O, (f) Fe, (g) Mo, (h) S, and (i) Ti.



For the ZDDP-based lubricants, PAO4_ZDDP produced a wear scar with distinct grooves and locally covered dark regions, as shown in Figs. 6a and 6b. At higher magnification, island-like or flake-like reaction products coexisted with exposed grooves, indicating that ZDDP-derived tribochemical products were formed but were heterogeneously distributed. The EDS results in Fig. 6c confirm the presence of Zn, P, and S, with contents of 0.68 wt%, 0.24 wt%, and 0.37 wt%, respectively. However, the Fe content remained high at 89.09 wt%, suggesting that the ZDDP-derived tribofilm did not provide continuous coverage over the steel substrate. The weak and dispersed Zn, P, and S signals in Figs. 6d–6i further indicate limited film continuity under this condition.

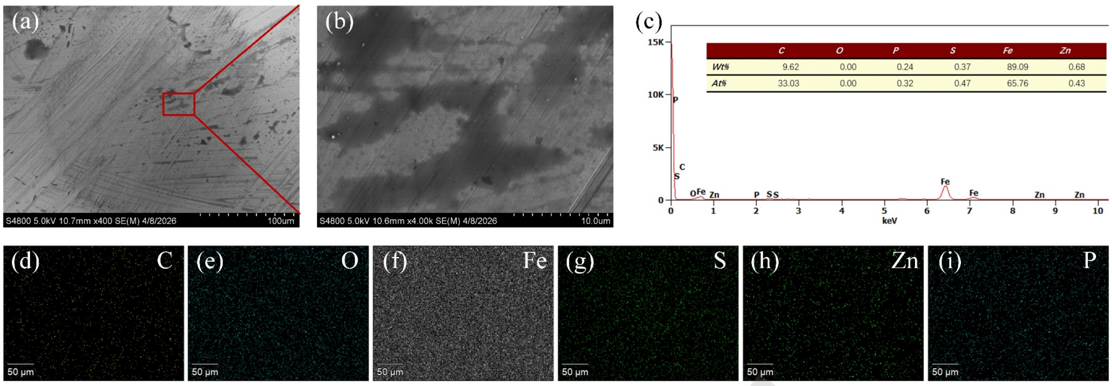


**Fig. 6**. SEM images of the wear scar surface on the steel ball lubricated with PAO4_ZDDP under a normal load of 20 N. (a) low-magnification and (b) high-magnification SEM images; (c) elemental contents in the wear scar region shown in (b); and corresponding EDS elemental maps of (d) C, (e) O, (f) Fe, (g) S, (h) Zn, and (i) P.

In contrast, the ZDDP_$TiO_2$-lubricated surface showed improved morphological uniformity after the introduction of $TiO_2$ nanoparticles, as shown in Figs. 7a and 7b. Although sliding-direction grooves were still present, large adhered debris, severe local accumulation, and obvious spalling were reduced. The surface was mainly characterized by relatively dense stripe-like marks and finely dispersed particulate features, suggesting a more stable interfacial state during sliding. The detection of Ti together with Zn-, P-, and S-containing species in Figs. 7c–7j suggests the involvement of Ti-containing species in the interfacial process. Compared with PAO4_ZDDP, $TiO_2$ did not completely eliminate abrasive features, but it reduced local damage and improved the uniformity of the wear scar. This suggests that $TiO_2$ can moderately regulate ZDDP-derived tribofilm formation, although its promoting effect was less significant than that observed in MoDTC_$TiO_2$.

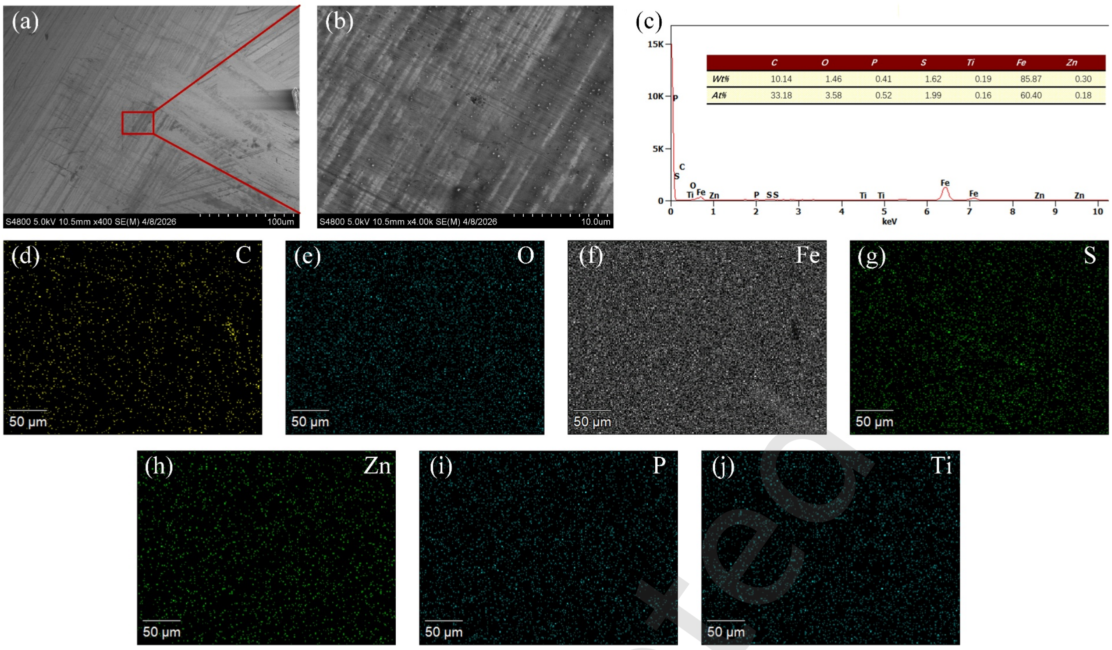


**Fig. 7**. SEM images of the wear scar surface on the steel ball lubricated with ZDDP_$TiO_2$ under a normal load of 20 N. (a) low-magnification and (b) high-magnification SEM images; (c) elemental contents in the wear scar region shown in (b); and corresponding EDS elemental maps of (d) C, (e) O, (f) Fe, (g) S, (h) Zn, (i) P, and (j) Ti.

For the blended additive systems, MoDTC_ZDDP produced a relatively smooth wear scar with mild grooves and locally covered regions, as shown in Fig. 8a and b. No severe spalling or large-scale adhesive damage was observed, indicating that the combined use of MoDTC and ZDDP contributed to the formation of a relatively stable interfacial layer. The EDS results in Fig. 8c show the simultaneous presence of Mo, S, Zn, and P, with contents of 0.15 wt%, 0.29 wt%, 0.47 wt%, and 0.11 wt%, respectively. The elemental maps in Figs. 8d–8j further confirm that both MoDTC and ZDDP participated in tribofilm formation. Although the overall contents of these active elements were relatively low, their coexistence suggests the formation of a composite tribofilm containing both MoDTC- and ZDDP-derived reaction products.

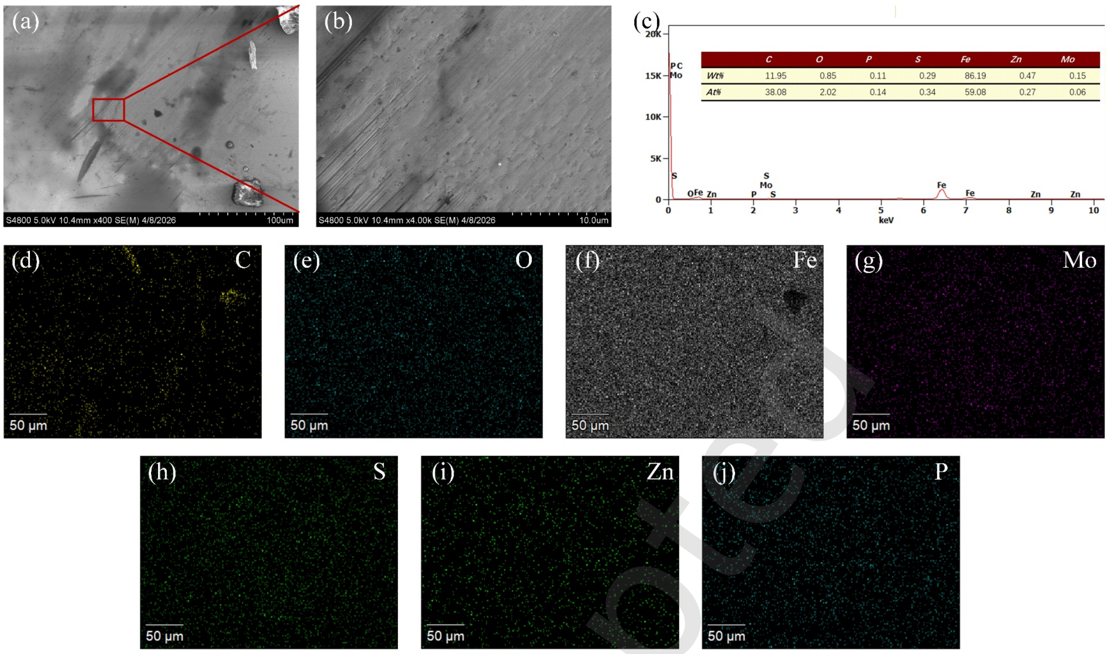


**Fig. 8**. SEM images of the wear scar surface on the steel ball lubricated with MoDTC_ZDDP under a normal load of 20 N. (a) low-magnification and (b) high-magnification SEM images; (c) elemental contents in the wear scar region shown in (b); and corresponding EDS elemental maps of (d) C, (e) O, (f) Fe, (g) Mo, (h) S, (i) Zn, and (j) P.



However, the addition of $TiO_2$ to MoDTC_ZDDP did not further improve the wear scar morphology or active-element enrichment. As shown in Fig. 9a and b, the MoDTC_ZDDP_$TiO_2$-lubricated surface still exhibited obvious grooves and local particulate adhesion, without forming a more compact or continuous protective film. The EDS results in Fig. 9c show that the Fe content remained high at 88.82 wt%, while the Mo, S, Zn, P, and Ti signals were weak and scattered. The elemental maps in Fig. 9d-k further confirm the absence of pronounced enrichment of active tribofilm-forming elements. These results indicate that although $TiO_2$ nanoparticles were involved in the interfacial process, they did not effectively enhance the formation or continuity of the composite tribofilm in the MoDTC_ZDDP blended system.

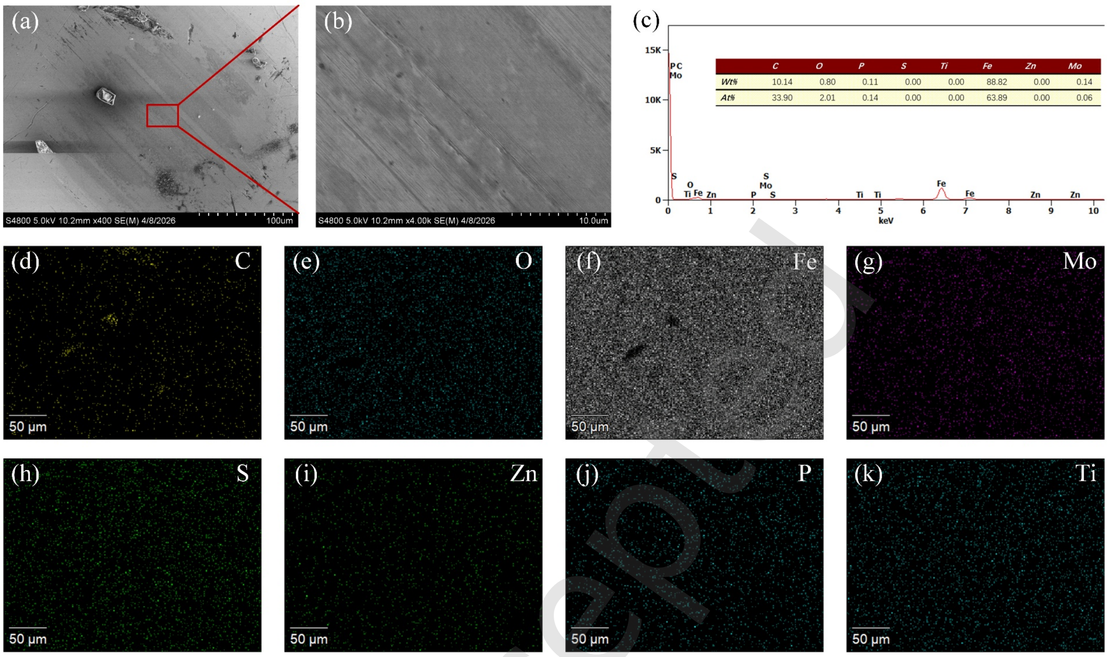


**Fig. 9**. SEM images of the wear scar surface on the steel ball lubricated with MoDTC_ZDDP_$TiO_2$ under a normal load of 20 N. (a) low-magnification and (b) high-magnification SEM images; (c) elemental contents in the wear scar region shown in (b); and corresponding EDS elemental maps of (d) C, (e) O, (f) Fe, (g) Mo, (h) S, (i) Zn, (j) P, and (k) Ti.

Overall, the SEM/EDS results in Figs. 4–9 demonstrate that the role of $TiO_2$ nanoparticles is strongly formulation-dependent. In MoDTC-containing lubricants, $TiO_2$ significantly promoted the enrichment of Mo- and S-containing species and improved tribofilm coverage. In ZDDP-containing lubricants, $TiO_2$ moderately improved wear scar uniformity and reduced local surface damage. In contrast, in MoDTC-ZDDP blended lubricants, $TiO_2$ did not further enhance active-element enrichment or tribofilm continuity. This suggests that the beneficial effect of $TiO_2$ may be weakened in multi-additive formulations, likely due to competitive adsorption and tribochemical interactions among MoDTC, ZDDP, and $TiO_2$ nanoparticles.

### *3.3 Chemical composition of tribofilm*

To further elucidate the tribochemical characteristics of tribofilms formed by different lubricants at 20 N, representative samples from the wear scars on the steel balls tested at 20 N were selected for XPS analysis. Particular attention was paid to the peak deconvolution of the Mo 3d and S 2p high-resolution spectra. By comparing the valence-state distribution of Mo and the chemical-state evolution of S among different lubricants, the decomposition and transformation behavior of MoDTC during sliding can be further identified. In addition, the regulatory effects of $TiO_2$ nanoparticles and ZDDP on the tribochemical reactions of MoDTC can be clarified. During data processing, all XPS spectra were calibrated by referencing the C–C component of the C 1s peak to 284.8 eV, while peak fitting and quantitative analysis were performed using PHI MultiPak software. By comparing the surface chemical states of the tribofilms, important insights can be obtained into the formation mechanism, structural evolution, and friction- and wear-reduction functions of the tribofilms generated during the synergistic lubrication processes involving MoDTC, ZDDP, and $TiO_2$ nanoparticles.

High-resolution XPS spectra of Mo 3d and S 2p were used to analyze the friction-induced changes in chemical states, as shown in Figs. 10 and 11. According to the peak-fitting results, the Mo 3d spectra can be mainly assigned to three chemical valence states, namely $Mo^{6+}$, $Mo^{4+}$, and $Mo^{2+}$, with corresponding binding energies of 232.2 ± 0.2 eV, 229.0 ± 0.2 eV, and 228.2 ± 0.2 eV, respectively. Based on previous studies on the tribochemical decomposition mechanism of MoDTC, $Mo^{6+}$ is mainly associated with $MoO_3$, whereas $Mo^{4+}$ can be attributed primarily to $MoS_2$ and/or $MoO_2$. The S 2p spectra can be mainly assigned to two sulfur-containing chemical species, namely $MoS_2$ and $SO_4^{2-}$, with corresponding binding energies of 163.4 ± 0.2 eV and 167.8 ± 0.2 eV, respectively. In addition, to improve the accuracy of spectral fitting, the corresponding satellite peaks were also fitted and presented. Meanwhile, the S 2s peak located at 226 ± 0.2 eV provides further evidence for the formation of sulfur-containing tribochemical products.

Under PAO4_MoDTC lubrication, the high-resolution Mo 3d spectrum of the tribofilm formed on the steel ball wear scar showed that the relative peak area fractions of $Mo^{6+}$, $Mo^{4+}$, and S 2s were 70.98%, 21.51%, and 7.51%, respectively (Figs. 10a and 10e). The dominant $Mo^{6+}$ component indicates that the tribofilm formed under this condition contained a relatively high proportion of $MoO_3$-related reaction products. In contrast, after the incorporation of $TiO_2$ nanoparticles, the corresponding fractions of $Mo^{6+}$, $Mo^{4+}$, and S 2s were 45.17%, 45.22%, and 9.60%, respectively (Figs. 10b and 10e). This result indicates that, under the 20 N load, $TiO_2$ nanoparticles promoted the conversion of MoDTC-derived Mo species from $Mo^{6+}$ to $Mo^{4+}$, thereby facilitating the formation of more $MoS_2$-containing tribofilms and leading to improved lubrication performance.

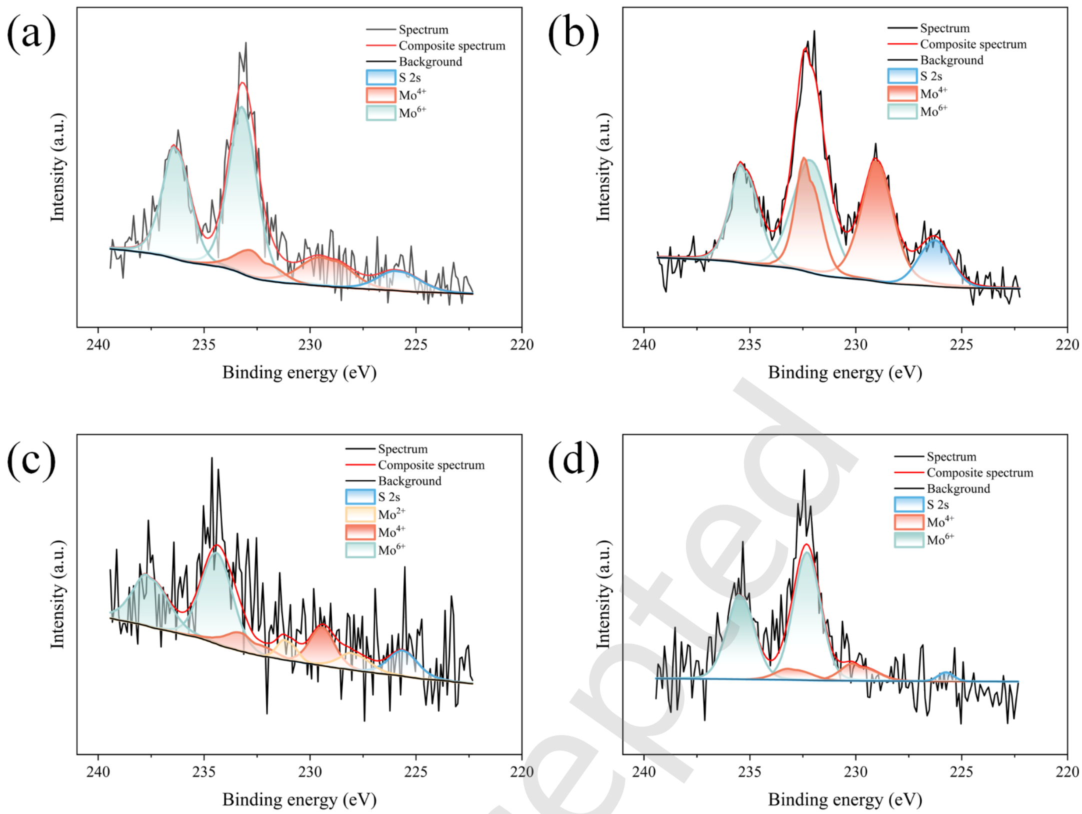


(e)

| | S 2s | $Mo^{2+}$ | $Mo^{4+}$ | $Mo^{6+}$ |
|---|---|---|---|---|
| MoDTC | 7.51% | - | 21.51% | 70.98% |
| MoDTC_$TiO_2$ | 9.60% | - | 45.22% | 45.17% |
| MoDTC_ZDDP | 9.65% | 11.14% | 20.68% | 58.44% |
| MoDTC_ZDDP_$TiO_2$ | 1.96% | - | 13.13% | 84.92% |

**Fig. 10**. High-resolution XPS Mo 3d spectra acquired from the wear scar surfaces of steel balls under a normal load of 20 N. (a) PAO4_MoDTC, (b) MoDTC_$TiO_2$, (c) MoDTC_ZDDP, and (d) MoDTC_ZDDP_$TiO_2$; (e) quantitative analysis of the relative peak area fractions corresponding to different chemical states.

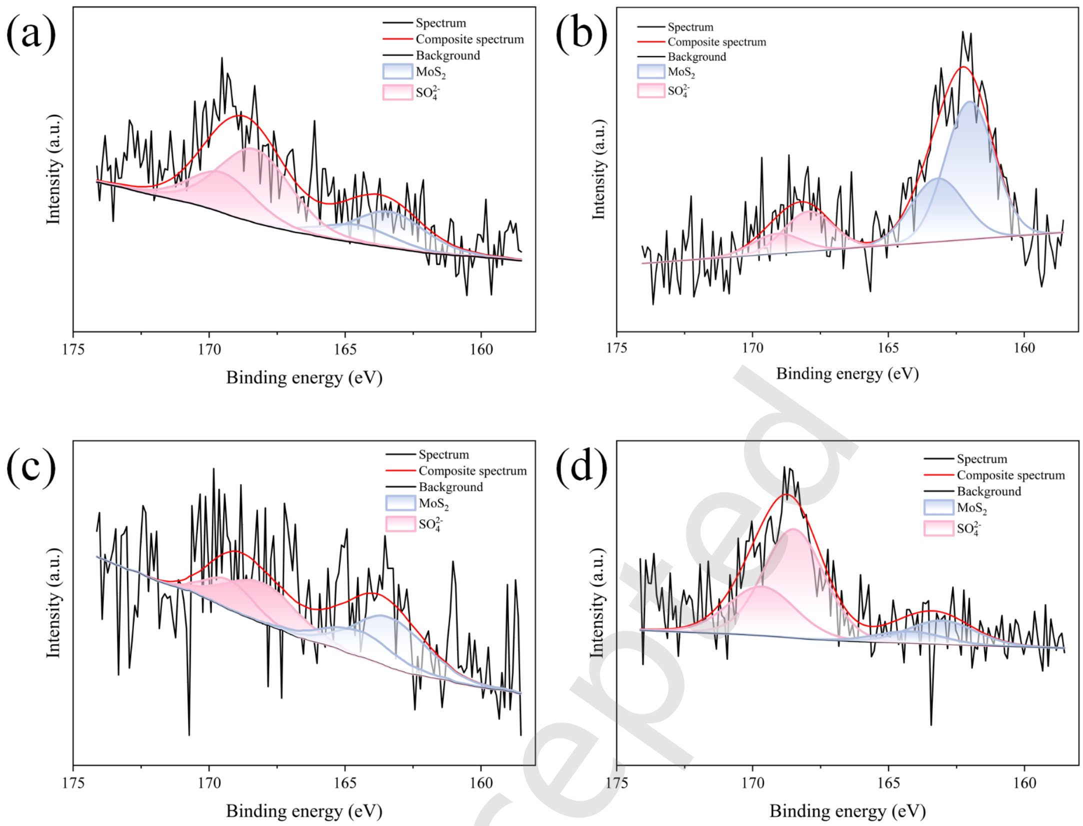


(e)

| | $MoS_2$ | $SO_4^{2-}$ |
|---|---|---|
| MoDTC | 33% | 67% |
| MoDTC_TiO$_2$ | 77.61% | 22.39% |
| MoDTC_ZDDP | 57.48% | 42.52% |
| MoDTC_ZDDP_TiO$_2$ | 19.44% | 80.56% |

**Fig. 11**. High-resolution XPS S 2p spectra acquired from the wear scar surfaces of steel balls under a normal load of 20 N. (a) PAO4_MoDTC, (b) MoDTC_TiO$_2$, (c) MoDTC_ZDDP, and (d) MoDTC_ZDDP_TiO$_2$; (e) quantitative analysis of the relative peak area fractions corresponding to different chemical states.

Under MoDTC_ZDDP lubrication, the high-resolution Mo 3d spectrum of the tribofilm formed on the steel ball wear scar showed that the relative peak area fractions of $Mo^{6+}$, $Mo^{4+}$, and S 2s were 58.44%, 20.68%, and 9.65%, respectively. In addition, a $Mo^{2+}$

component appeared, accounting for 11.14% of the total peak area (Figs. 10c and 10e). Compared with PAO4_MoDTC, the chemical-state composition of Mo in the MoDTC_ZDDP was more complex, involving not only high-valence oxides and intermediate-valence Mo species but also lower-valence Mo components. This indicates that, under the 20 N load, ZDDP exerted a regulatory effect on the interfacial reaction of MoDTC; however, it did not drive the tribofilm toward a $MoS_2$-dominated structure.

Under MoDTC_ZDDP_$TiO_2$ lubrication, the relative peak area fractions of $Mo^{6+}$, $Mo^{4+}$, and S 2s in the tribofilm were 84.92%, 13.13%, and 1.96%, respectively (Figs. 10d and 10e). This result indicates that the proportion of $Mo^{4+}$ decreased markedly when MoDTC, ZDDP, and $TiO_2$ nanoparticles acted simultaneously. Therefore, the role of $TiO_2$ nanoparticles varies significantly among different blended lubricants. In the MoDTC_$TiO_2$ system, $TiO_2$ nanoparticles facilitated the tribochemical decomposition of MoDTC toward the formation of more $MoS_2$-containing species. In contrast, in the MoDTC-ZDDP blended system, the incorporation of $TiO_2$ nanoparticles promoted the predominance of Mo species in the form of $MoO_3$-related products within the tribofilm.

Chemical states of phosphorus-containing and sulfur-containing tribochemical products in different lubricants were further analyzed. With the lubrication of MoDTC_ZDDP, the P 2p spectrum has a peak corresponding to phosphate [33], while with the lubrication of MoDTC_ZDDP_$TiO_2$, the P 2p spectrum has no obvious peaks

(Fig. S1). Fig. 11 presents the fitted S 2p spectra acquired from the wear scar surfaces of the steel balls under a normal load of 20 N. The S 2p spectra mainly consist of two sulfur species, namely $MoS_2$ and $SO_4^{2-}$. Among them, $MoS_2$ represents an important low-shear lubricating phase generated from the tribochemical decomposition of MoDTC, whereas $SO_4^{2-}$ corresponds to oxidized sulfur-containing products formed during the sliding process. Moreover,

Under PAO4_MoDTC lubrication, the relative peak area fractions corresponding to $MoS_2$ and $SO_4^{2-}$ in the tribofilm were 33% and 67%, respectively (Figs. 11a and 11e). This indicates that, under the 20 N load, sulfur-containing species in the tribofilm formed by the single MoDTC additive were dominated by oxidized sulfur species, whereas the proportion of sulfide-type lubricating phases represented by $MoS_2$ was relatively low. Combined with the Mo 3d results in Fig. 10a, these findings suggest that the tribofilm formed by PAO4_MoDTC under the 20 N load exhibited a pronounced oxidized character overall, with both Mo and S tending to exist in higher oxidation states. In contrast, after the incorporation of $TiO_2$ nanoparticles, the S 2p spectral distribution of MoDTC_$TiO_2$ changed significantly, with the relative peak area fractions of $MoS_2$ and $SO_4^{2-}$ reaching 77.61% and 22.39%, respectively (Figs. 11b and 11e). Compared with PAO4_MoDTC, $TiO_2$ nanoparticles markedly promoted the decomposition of MoDTC toward $MoS_2$ formation.

For MoDTC_ZDDP, the relative peak area fractions of $MoS_2$ and $SO_4^{2-}$ were 57.48% and 42.52%, respectively (Figs. 11c and 11e). Compared with PAO4_MoDTC, the proportion of $MoS_2$ increased markedly, while that of $SO_4^{2-}$ decreased, indicating that the combination of MoDTC and ZDDP enhanced interfacial sulfidation to some extent. Nevertheless, sulfate species still accounted for a considerable proportion, suggesting that sulfur in this system was not fully enriched in the form of sulfides but underwent significant oxidative transformation simultaneously. Under MoDTC_ZDDP_$TiO_2$ lubrication, the relative peak area fractions of $MoS_2$ and $SO_4^{2-}$ were 19.44% and 80.56%, respectively (Figs. 11d and 11e). This indicates that, under the combined action of ZDDP and $TiO_2$ nanoparticles, sulfur species at the friction interface existed predominantly in the form of sulfates, while sulfide formation was markedly suppressed. Combined with the results in Fig. 10d, it can be inferred that the tribofilm formed on the steel ball surface was mainly composed of high-valence molybdenum oxides and sulfate species. Considering that ZDDP can decompose during sliding to generate sulfur- and phosphorus-containing reaction products and participate in the construction of surface films, these results suggest that, under the present test conditions, the sulfur-containing oxidized products derived from ZDDP decomposition played a more dominant role in determining the interfacial sulfur chemistry. The incorporation of $TiO_2$ further altered the surface reaction pathway, causing sulfur to preferentially exist in a stable sulfate form rather than as $MoS_2$.

Overall, Figs. 10 and 11 demonstrate that different lubricants exert markedly different effects on the chemical states of tribofilms formed on the steel ball surfaces under the 20 N load. From the perspective of tribochemistry, the binary combination of $TiO_2$ nanoparticles with MoDTC is more favorable for forming low-valence, sulfur-containing tribofilms with potential friction-reducing capability. In contrast, the simultaneous incorporation of ZDDP and $TiO_2$ nanoparticles drives the interfacial reactions preferentially toward oxidation and sulfate formation. These results indicate that the synergistic effect of ZDDP on MoDTC does not necessarily promote $MoS_2$ formation under all operating conditions. Instead, its actual influence is jointly governed by the applied load, interfacial environment, and the participation mode of the third component, namely $TiO_2$ nanoparticles. This conclusion provides an essential chemical basis for further discussing the lubrication mechanisms of different lubricants in relation to their friction coefficient and wear results.

### *3.4 Analysis of microscale friction behavior of the tribofilm surfaces*

To quantitatively characterize the microscale tribological behavior of tribofilm surfaces formed by different lubricants, AFM was employed to perform friction force measurements on the worn surfaces. In addition, the corresponding surface morphology was also obtained using AFM to understand the relation between tribofilm formation and lubrication behavior.

Fig. 12 presents the surface topographies and corresponding friction force distribution maps of the tribofilms formed on the steel balls. Unlike macroscopic tribological tests, AFM-based microscale friction measurements reflect the local interaction between the probe and the tribofilm surface. Therefore, by comparing the correlation between surface topography and friction force distribution, the influence of tribofilm formation process on the tribological behaviors can be further analyzed. For the tribofilm formed under MoDTC_$TiO_2$ lubrication, a clear inverse correspondence was observed locally between surface height and friction force, as shown in Figs. 12c and 12d. Taking the marked regions A and B as examples, region A corresponded to a relatively protruded area in the topography image but exhibited a lower friction force in the corresponding friction map. In contrast, region B was located at a relatively lower position in the topography image, yet showed a higher local friction force. This phenomenon indicates that the local friction behavior of the MoDTC_$TiO_2$ tribofilm was closely related to the local composition and shear characteristics of the tribofilm.

Combined with the above XPS results, the relatively high proportion of $MoS_2$ in the MoDTC_$TiO_2$ system suggests that $TiO_2$ nanoparticles promoted the decomposition of MoDTC to form low-shear Mo-containing tribochemical films. Therefore, the regions with greater topographic height may correspond to tribofilm domains enriched in $MoS_2$ or similar tribochemical products. Although these regions were topographically higher, their intrinsically low interlayer shear strength resulted in lower local shear resistance during probe scanning. By contrast, the lower-lying regions may correspond to insufficient tribofilm formation, local wear, or substrate exposure, leading the probe to interact with a harder surface or a discontinuous film and thereby generating a higher friction force.

Compared with $MoDTC\_TiO_2$, $MoDTC\_ZDDP\_TiO_2$ exhibited markedly different microscale friction behavior. As shown in Figs. 12e and 12f, a certain positive correlation between surface height and friction force was observed on the wear scar surface lubricated with $MoDTC\_ZDDP\_TiO_2$. Taking regions C and D as examples, region C was located at a relatively lower position in the topography image and correspondingly showed a lower friction force. In contrast, region D appeared as a relatively elevated area in the topography image and also exhibited a higher friction force.

This result indicates that, in the wear region lubricated with $MoDTC\_ZDDP\_TiO_2$, the protruded surface regions were not enriched with low-shear lubricating phases, but were more likely associated with hard tribochemical products, oxides, or salt-like species. These regions could increase the local contact resistance during AFM probe scanning, thereby resulting in higher friction forces. Conversely, the lower-lying regions may have been relatively smoother or contained fewer deposited reaction products, leading to reduced resistance during probe sliding and thus lower local friction forces. The result is in good agreement with the XPS analysis. In the $MoDTC\_ZDDP\_TiO_2$ system, the proportions of $Mo^{6+}$ and $SO_4^{2-}$ increased markedly, whereas the proportion of $MoS_2$ decreased, indicating that after the incorporation of $TiO_2$ nanoparticles, the surface tribofilm formed under the MoDTC-ZDDP blended lubricant tended to evolve toward enrichment in high-valence oxides and sulfate species. Although these products may possess a certain degree of chemical stability, they do not exhibit the low-shear characteristics associated with the layered structure of $MoS_2$. When such species exist on the surface in the form of local protrusions or non-uniform deposits, they can increase the local resistance experienced by the AFM probe during sliding, thereby producing a correspondence in which elevated topographic regions exhibit higher friction forces, while lower regions show lower friction forces. This suggests that the tribofilm formed under MoDTC_ZDDP_$TiO_2$ lubrication is not a typical low-shear tribofilm, but is more likely a composite tribofilm containing oxide- and sulfate-rich components, with relatively limited local friction-reducing capability.

Overall, Fig. 12 demonstrates that the tribofilms formed by different lubricants exhibited markedly different local friction behavior at the microscale. In the MoDTC_$TiO_2$, the topographically elevated regions corresponded to lower friction forces, suggesting that these protruded regions may have been enriched with low-shear $MoS_2$-derived products and thus possessed favorable local friction-reducing capability. In contrast, in the MoDTC_ZDDP_$TiO_2$, the elevated regions corresponded to higher friction forces, indicating that the protrusions were more likely derived from high-friction reaction products or local deposits rather than effective low-shear lubricating phases.

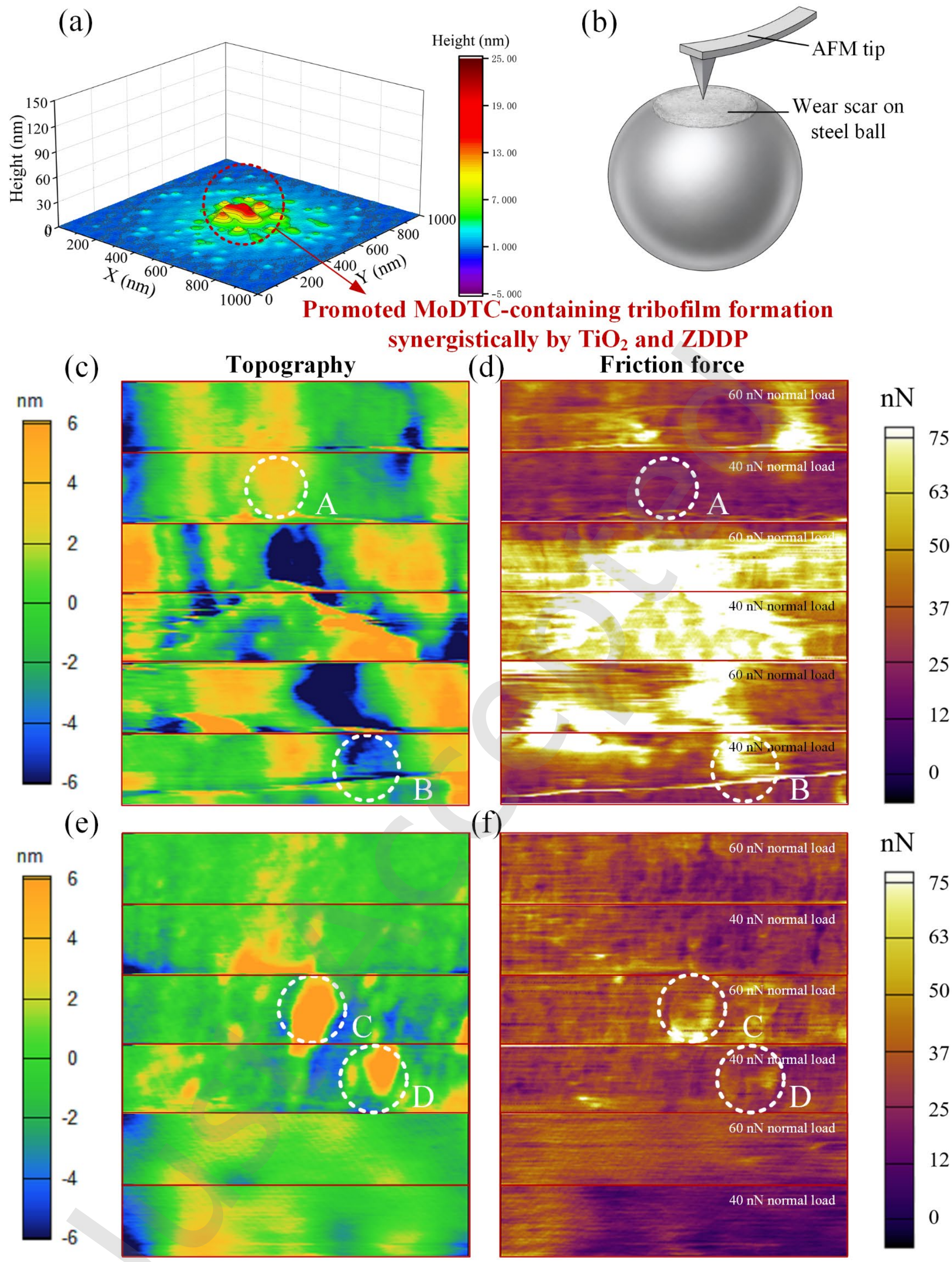


**Fig. 12**. Microscale friction measurements of tribofilm surfaces on steel balls lubricated with different formulations. (a) Schematic illustration of the tribofilm surface morphology and (b) schematic illustration of the AFM measurement. Tribofilm surface topographies of (c) MoDTC_$TiO_2$ and (d) MoDTC_ZDDP_$TiO_2$, and corresponding friction force distribution maps of (e) MoDTC_$TiO_2$ and (f) MoDTC_ZDDP_$TiO_2$. The tribofilm surfaces were scanned over an area of 1 μm × 0.2 μm under normal loads of 40 and 60 nN, respectively. All the tests were repeated in 3 different regions.

### *3.5 Tribochemical synergistic mechanism of $TiO_2$ nanoparticle regulation in the MoDTC-ZDDP blended system*

MoDTC and ZDDP are representative friction modifier and anti-wear additive in lubricating oils. However, their functions in blended systems are not simply additive; rather, they are jointly governed by interfacial adsorption competition, differences in decomposition pathways, and the dynamic evolution of tribofilms. Therefore, elucidating the tribochemical reaction behavior of the MoDTC-ZDDP blended system and further clarifying the regulatory role of $TiO_2$ nanoparticles in this process are of great significance for achieving the synergistic optimization of friction reduction and wear protection.

By integrating the above results in this study, it can be concluded that $TiO_2$ nanoparticles can significantly enhance the lubrication and wear resistance performance of MoDTC, where the gradual reduction of COF during the running-in process when lubricated with MoDTC_$TiO_2$ and MoDTC_ZDDP_$TiO_2$ was attributed to the dynamic formation of tribofilm [34]. In addition, $TiO_2$ nanoparticles can also significantly affect the interfacial reaction pathways and tribofilm evolution process of the MoDTC-ZDDP blended system, which demonstrates that $TiO_2$ nanoparticles exert a clear regulatory effect on the tribochemical reactions of the blended additive system. However, the wear volume results shown in Fig. 3 indicate that, after the incorporation of $TiO_2$ nanoparticles, MoDTC_ZDDP_$TiO_2$ exhibited a markedly larger wear volume than MoDTC_ZDDP. This suggests that such regulation did not lead to further improvement in anti-wear performance under the present test conditions. Therefore, the role of $TiO_2$ nanoparticles in the MoDTC-ZDDP blended system cannot be simply described as a “beneficial” effect; rather, it should be regarded as a selective and complex interfacial regulatory effect.

From the perspective of surface chemical states, Figs. 10 and 11 show that, after the incorporation of $TiO_2$ nanoparticles, Mo species in the MoDTC_ZDDP_$TiO_2$ tribofilm existed predominantly as $Mo^{6+}$, while sulfur species were preferentially enriched as $SO_4^{2-}$. In contrast, the proportion of low-shear sulfur-containing species such as $MoS_2$ decreased markedly. This result indicates that $TiO_2$ nanoparticles altered the decomposition and transformation pathways of the MoDTC-ZDDP blended system at the friction interface, shifting the surface tribofilm from a state relatively enriched in low-valence Mo-containing active phases toward a surface structure dominated by high-valence Mo oxides and sulfate species.

From the perspective of microscale friction behavior, the AFM results further reveal distinct differences in the local shear characteristics of the tribofilms. As shown in Fig. 12, in the MoDTC_$TiO_2$ system, topographically elevated regions corresponded to lower friction forces, whereas lower regions exhibited higher friction forces. This suggests that the local protruded regions in MoDTC_$TiO_2$ were likely enriched in low-shear reaction products such as $MoS_2$. Although these regions were higher in surface topography, they generated lower shear resistance during probe sliding, thereby exhibiting favorable friction-reducing capability.

In contrast, MoDTC_ZDDP_$TiO_2$ displayed the opposite behavior, where topographically protruded regions corresponded to higher friction forces, while lower regions corresponded to lower friction forces. This indicates that the protruded regions in this system were not enriched with low-shear lubricating phases, but were more likely associated with high-valence oxides, sulfate deposits, or local accumulation of particles/reaction products. These regions increased the local contact resistance and shear resistance during AFM probe scanning, resulting in higher friction forces.

The AFM results are in good agreement with the XPS analysis. After $TiO_2$ nanoparticles were incorporated into the MoDTC-ZDDP blended system, the tribofilm composition was altered; however, the resulting surface products did not exhibit $MoS_2$-like low-shear characteristics. This further indicates that the $TiO_2$-regulated composite tribofilm did not outperform MoDTC_$TiO_2$ in terms of local friction-reducing capability, nor did it form an ideal composite film combining low shear strength with high wear resistance under the present test conditions.

In summary, the regulation of tribochemical reactions in the MoDTC-ZDDP blended system by $TiO_2$ nanoparticles is first reflected in their ability to enter the frictional contact region and participate in tribofilm formation. The detection of Ti signals in the

EDS results indicates that $TiO_2$ nanoparticles did not merely remain as free particles in the lubricant medium, but were involved in the construction of the surface film within the wear scar. Their presence may alter the local stress distribution, surface active sites, and adsorption/decomposition behavior of additive molecules at the contact interface, thereby influencing the tribochemical reactions of MoDTC and ZDDP.

Second, $TiO_2$ nanoparticles can alter the interfacial reaction pathways in the MoDTC-ZDDP blended system. For the single MoDTC-containing lubricant, $TiO_2$ nanoparticles promote the conversion of MoDTC into low-shear Mo-containing products such as $MoS_2$, thereby producing favorable synergistic friction-reducing and anti-wear effects. However, in the MoDTC-ZDDP blended system, ZDDP participates in the formation of reaction films containing elements such as Zn, P, and S, leading to a more complex interfacial reaction environment. The incorporation of $TiO_2$ nanoparticles further drives the surface film in the blended system toward enrichment in high-valence Mo oxides and sulfate species, thereby reducing the relative proportion of low-shear active components such as $MoS_2$.

In addition, the composite tribofilm formed after $TiO_2$ nanoparticle regulation failed to achieve an effective match between chemical composition and mechanical and shear properties. Although MoDTC_ZDDP_$TiO_2$ generated a multicomponent composite film, the enrichment of active elements in the surface layer was not pronounced, and the Fe signal remained strong. Meanwhile, the AFM results showed that local protruding regions corresponded to higher friction forces, indicating that this film did not exhibit the desired low-shear characteristics. Therefore, this system formed neither a sufficiently continuous and compact anti-wear protective layer nor a friction-reducing film dominated by low-shear components such as $MoS_2$.

Therefore, the role of $TiO_2$ nanoparticles in the MoDTC-ZDDP blended system is not simply to promote film formation or enhance lubrication, but rather to reconstruct the interfacial reaction pathways and the surface structure of the tribofilm. Under the present 20 N condition, this reconstruction drives the surface film toward greater enrichment in oxidized or salt-like products, such as $Mo^{6+}$ species and $SO_4^{2-}$. However, this type of film does not achieve an effective match with the low-shear friction-reducing capability and anti-wear protection required for the blended additive system, ultimately resulting in an increased wear volume.

## 4. Conclusion

This study systematically investigated the tribochemical and tribomechanical effects of $TiO_2$ nanoparticles on MoDTC and ZDDP additives, both individually and in combination. The results reveal that $TiO_2$ nanoparticles exert formulation-dependent regulatory effects on tribofilm formation and tribological performance, with distinct mechanisms operating in single-additive versus blended lubricant systems. Based on the results obtained in this work, the following conclusions can be drawn:

- $TiO_2$ nanoadditive exhibits formulation-dependent tribological effects. $TiO_2$

nanoparticles enhanced the friction-reducing performance of MoDTC and improved the anti-wear behavior of ZDDP. However, in the MoDTC-ZDDP blend, $TiO_2$ incorporation increased wear volume and prolonged running-in, demonstrating that nanoparticle regulation is not universally beneficial.

• $TiO_2$ nanoadditive promotes $MoS_2$ formation in MoDTC-$TiO_2$. XPS showed $TiO_2$ promoted MoDTC decomposition toward low-shear products. In high-resolution Mo 3d spectra, the content of $Mo^{4+}$ increased from 21.5% to 45.2%; and in high-resolution S 2p spectra, $MoS_2$ fraction rose from 33% to 77.6%. Meanwhile, AFM revealed an inverse topography-friction correlation, confirming that protruded regions were enriched with $MoS_2$-like low-shear phases.

• $TiO_2$ nanoadditive shifts oxidative pathway in MoDTC-ZDDP-$TiO_2$. In the blended system, $TiO_2$ drove reactions toward high-valence oxides. In high-resolution Mo 3d spectra, $Mo^{6+}$ reached 84.9%; and in high-resolution S 2p spectra, $SO_4^{2-}$ dominated sulfur chemistry (80.6%), with $MoS_2$ dropping to 19.4%. Meanwhile, AFM showed protruded regions corresponded to higher friction, indicating hard oxide/sulfate deposits rather than lubricating phases.

• $TiO_2$ leads to interfacial reaction network reconstruction. Elemental distribution at the contact surfaces confirmed Ti incorporation into tribofilms, indicating active participation in surface film construction. $TiO_2$ altered local stress distribution and active sites, redirecting the competition between sulfidation and oxidation pathways at the friction interface.

• The findings provide implications for the design of nanolubricants. The tribochemical synergy of $TiO_2$ is highly system-specific. While effective for single-MoDTC lubricants, its combination with ZDDP leads to oxidative product enrichment that compromises both friction and wear performance. Rational nanoparticle formulation design must account for additive interactions and interfacial reaction competition in multi-additive packages.

**Acknowledgements**

This work was financially supported by the National Natural Science Foundation of China (grant number 52475176), Beijing Natural Science Foundation (grant numbers L257026, L2611033), Hebei Natural Science Foundation (grant number E2024105063), and Young Elite Scientists Sponsorship Program by BAST (grant number BYESS2023288).

**References**

[1] J. Luo, X. Zhou, Superlubricitive engineering—Future industry nearly getting rid of wear and frictional energy consumption, Friction 8(4) (2020) 643-665.
[2] K. Holmberg, A. Erdemir, Influence of tribology on global energy consumption, costs and emissions, Friction 5(3) (2017) 263-284.
[3] J. Zhang, Y. Meng, Boundary lubrication by adsorption film, Friction 3(2) (2015) 115-147.
[4] Y. Xia, P. Cheng, J. Fei, W. Wang, J. Yan, Z. Hu, L. Qi, Enhanced tribological performance of environmentally friendly lubricants with CS/ZnO composite nanoparticles additives, Carbon 248 (2026) 121124.
[5] Z. Wu, J. Fei, C. Li, J. Yan, X. Ke, L. Qi, Effect of 2D Cu-MOFs modified carbon spheres nanoparticles as an environmentally friendly lubricating additive on tribological properties, Tribology International 192 (2024) 109321.
[6] J. Qu, H. Luo, M. Chi, C. Ma, P.J. Blau, S. Dai, M.B. Viola, Comparison of an oil-miscible ionic liquid and ZDDP as a lubricant anti-wear additive, Tribology International 71 (2014) 88-97.
[7] N. Wang, H. Wang, J. Ren, G. Gao, G. Zhao, Y. Yang, J. Wang, High-efficient and environmental-friendly PTFE@$SiO_2$ core-shell additive with excellent AW/EP properties in PAO6, Tribology International 158 (2021) 106930.
[8] J. Wang, T. He, C. Song, X. Li, B. Chen, Engine Oil Degradation Induced by Biodiesel: Effect of Methyl Oleate on the Performance of Zinc Dialkyldithiophosphate, ACS Omega 4(14) (2019)

16166-16170.
[9] Y. Liu, X. Ge, J. Li, Graphene lubrication, Applied Materials Today 20 (2020) 100662.
[10] X. Ge, Z. Chai, Q. Shi, Y. Liu, W. Wang, Graphene superlubricity: A review, Friction 11 (2023) 1953–1973.
[11] Y. Liu, S. Yu, J. Li, X. Ge, Z. Zhao, W. Wang, Quantum dots of graphene oxide as nano-additive triggers macroscale superlubricity with an extreme short running-in period, Materials Today Nano 18 (2022) 100219.
[12] S. Yi, J. Li, Y. Liu, X. Ge, J. Zhang, J. Luo, In-situ formation of tribofilm with $Ti_3C_2T_x$ MXene nanoflakes triggers macroscale superlubricity, Tribology International 154 (2021) 106695.
[13] M. Ivanov, O. Shenderova, Nanodiamond-based nanolubricants for motor oils, Current Opinion in Solid State and Materials Science 21(1) (2017) 17-24.
[14] Y. Liu, S. Yu, R. Zhang, X. Ge, W. Wang, "Non-layered" two-dimensional nanodiamond plates as nanoadditives in water lubrication, Wear 536-537 (2024) 205174.
[15] W. Zhai, K. Zhou, Nanomaterials in Superlubricity, Advanced Functional Materials 29(28) (2019) 1806395.
[16] Y.Y. Wu, W.C. Tsui, T.C. Liu, Experimental analysis of tribological properties of lubricating oils with nanoparticle additives, Wear 262(7) (2007) 819-825.
[17] Z. Fan, S. Wang, Y. Xiang, Y. Liu, Z. Yu, X. Ge, W. Wang, Synergetic lubrication between MoDTC and $TiO_2$ nano-additive: Dynamic evolution of tribofilm induced by tribocatalysis and tribomechanical effect, Tribology International 207 (2025) 110608.
[18] S. Kumar, R. Kumar, Tribological characteristics of synthesized hybrid nanofluid composed of CuO and $TiO_2$ nanoparticle additives, Wear 518-519 (2023) 204623.
[19] Z. Jiang, Y. Sun, B. Liu, L. Yu, Y. Tong, M. Yan, Z. Yang, Y. Hao, L. Shangguan, S. Zhang, W. Li, Research progresses of nanomaterials as lubricant additives, Friction 12(7) (2024) 1347-1391.
[20] K. Zeng, L. Cheng, S. Fan, C. Xu, R. Qu, X. Song, L. Da, W. Hu, J. Li, Surface functionalization strategy of $TiO_2$ nanoparticles governs nanofluid stability and lubrication, Tribology International 216 (2026) 111594.
[21] H. Spikes, The History and Mechanisms of ZDDP, Tribology Letters 17(3) (2004) 469-489.
[22] H. Spikes, Mechanisms of ZDDP—An Update, Tribology Letters 73(1) (2025) 38.
[23] J. Ruiz-Acero, F. Kessler, H. Costa, T. Cousseau, The effect of ethanol fuel dilution on oil performance and MoDTC tribofilms formation and composition, Friction 12(9) (2024) 2108-2125.
[24] H. Qiu, W. Hu, J. Liu, L. Li, S. Jiang, K. Bao, S. Han, J. Yan, Study on the synergy of nitrogen-containing borate ester organomolybdenum additives combined with ZDDP, Surface and Coatings Technology 522 (2026) 133152.
[25] D.N. Khaemba, A. Neville, A. Morina, New insights on the decomposition mechanism of Molybdenum DialkyldiThioCarbamate (MoDTC): a Raman spectroscopic study, RSC Advances 6(45) (2016) 38637-38646.
[26] Y. Liu, Z. Fan, S. Yu, R. Zhang, J. Zhang, T.W. Liskiewicz, X. Ge, W. Wang, Macroscale structural superlubricity: Dynamic evolution of tribolayers in two-dimensional materials under extreme pressure, Nano Energy 129 (2024) 110072.
[27] C. Espejo, C. Wang, B. Thiébaut, C. Charrin, A. Neville, A. Morina, The role of MoDTC tribochemistry in engine tribology performance. A Raman microscopy investigation, Tribology International 150 (2020) 106366.
[28] Z. Jiang, Z. Zhang, A. Jiang, Z. Yang, L. Yu, I.N. Kavaliova, M.V. Prozhega, Y. Hao, $MoS_2$

nanoadditives for lubrication: Morphology, surface chemistry, and mechanisms, Tribology International 214 (2026) 111151.
[29] T. Onodera, Y. Morita, A. Suzuki, R. Sahnoun, M. Koyama, H. Tsuboi, N. Hatakeyama, A. Endou, H. Takaba, C.A. Del Carpio, M. Kubo, T. Shin-yoshi, N. Nishino, A. Suzuki, A. Miyamoto, A Theoretical Investigation on the Dynamic Behavior of Molybdenum Dithiocarbamate Molecule in the Engine Oil Phase, Tribology Online 3(2) (2008) 80-85.
[30] A. Morina, A. Neville, M. Priest, J.H. Green, ZDDP and MoDTC interactions in boundary lubrication—The effect of temperature and ZDDP/MoDTC ratio, Tribology International 39(12) (2006) 1545-1557.
[31] S. Du, W. Yue, Y. Wang, D. She, H. Huang, Z. Fu, Synergistic effects between sulfurized-nanocrystallized 316L steel and MoDTC lubricating oil additive for improvement of tribological performances, Tribology International 94 (2016) 530-540.
[32] R. Unnikrishnan, M.C. Jain, A.K. Harinarayan, A.K. Mehta, Additive–additive interaction: an XPS study of the effect of ZDDP on the AW/EP characteristics of molybdenum based additives, Wear 252(3) (2002) 240-249.
[33] H.L. Costa, K.S. Evangelista, T. Cousseau, J.S.R. Acero, F. Kessler, Use of XANES and XPS to investigate the effects of ethanol contamination on anti-wear ZDDP tribofilms, Tribology International 159 (2021) 106997.
[34] H. Wu, J. Zhao, X. Cheng, W. Xia, A. He, J.-H. Yun, S. Huang, L. Wang, H. Huang, S. Jiao, Z. Jiang, Friction and wear characteristics of $TiO_2$ nano-additive water-based lubricant on ferritic stainless steel, Tribology International 117 (2018) 24-38.